International Academy of Science, Engineering and Technology
Connecting Researchers; Nurturing Innovations
IASET

MOHOROVICIC DISCONTINUITY BELOW THE CENTRAL INDIAN OCEAN BASIN DEFORMATION ZONE AS INFERRED FROM GRAVITY MODELLING.

M.SUBRAHMANYAM[1], S. RAJENDRAN[2] & T.K.S. PRAKASARAO[1]

[1]Department of Geophysics, Andhra University, Visakhapatnam-530 003, India

[2]School of Marine Sciences, Cochin University of Science & Technology, Cochin, India

ABSTRACT

The equatorial region of the Central Indian Ocean Basin (CIOB) is undergoing tectonic deformation since late Miocene age as a result of continued ocean floor spreading across the South East Indian Ridge and the resistance of shortening across the Himalaya. An attempt has been made here to study the deeper crustal structure based on gravity modeling. For this, two N-S and one E-W trending gravity profiles have been interpreted in terms of a three-layer density distribution using the densities determined from an empirical density versus seismic velocity curve compiled from various sources by Nafe and .Drake (1963). The velocity model for intensely folded and fractured anticlinal basement rise near 4^0S and 80^0E (Fig.8c of Neprochnov et al., 1988) is considered as one of the inputs for modeling the free-air anomaly profiles and to map the Moho underlying the deformation zone. The layer characterized by P wave velocity of 7.6km/sec, referred to as thickness of the crust up to discontinuity (or unconsolidated upper mantle?) by Neprochnov et al.,(1988), was considered in the present study as comprising of two layers or underplating material of variable density, 3.14g/cc to 3.24g/cc resulting from serpentinisation.

KEYWORDS: Miocene Age, Earthquake Source Mechanisms, Indian Ocean.

INTRODUCTION

Geological and geophysical studies in the recent times have suggested that the deformation of the Indian Ocean equatorial region has been active tectonically since the late Miocene after the Indian plate collided with the Eurasian plate. Two sets of folds are generally observed in the deformation zone. They are (i) long wavelength (100 – 300km) anticlinal basement structures with 1-2 km relief in the basement and overlying sediments and (ii) short wavelength undulations ranging from 5 to 20 km, generally occurring over the crests of the long wavelength anticlines. The short wavelength folds are bounded by high angle faults imparting an appearance of folded and faulted blocks separated by non-deformed strata.

Stratigraphic interpretation of seismic horizons made seismic methods a powerful tool in modeling shallow crustal structure. Deeper crust can be visualiased by gravity modeling. Although depth to the top of the source is a parameter of primary importance in geophysical situations, in certain geological situations, depth to the bottom of magnetic sources is sought. This can correspond to the

depth to the Curie temperature isotherm or a litho logic change. An attempt has been made in this paper to study the deeper crustal structure based on gravity modeling. For this, two-N-S trending gravity profiles along 79^0E and 81^0E longitudes between 1^0S and 13^0S latitudes and one E-W profiles along 7^0S latitude between 74^0 30'E and 80^0E longitudes have been interpreted in terms of a three-layer density distribution using the correlation of observed seismic velocities with mean Nafe-Drake curve. Neprochnov et al., (1988) indicated the layer of 7.6km/sec P wave velocity as the thickness of the crust upto discontinuity (or unconsolidated upper mantle ?). This composite material with densities intermediate between the overlying oceanic crust and the underlying mantle is considered in the present investigation as two layers or underplating material because P-wave velocities of 7.2 to 7.6 km/sec correspond to 3.14g/cc to 3.24g/cc density material suggesting serpentinisation.

SEISMIC WAVE VELOCITIES AND INFERED 3-LAYER DENSITY DISTRIBUTION

The frame-work of the CIOB area is inhomogeneous and is characterized by extremely deformed crustal blocks that are conspicuous against weaker and more monotonous deformation of sediments and basement. Regional seismic reflection profiles obtained on R/V "Dmitry Mendeleev" Cruise 31 supplied seismic records that revealed a great variety of fault blocks. (Neprochnov et al., 1988 quoting Levchenko et al., 1985). The crustal structure of the CIOB was also investigated using Ocean Bottom Seismographs at two sites during R/V "Dmitry Mendeleev" cruise 31 and obtained seismic reflection data. This data has been used in the present study to infer density distribution and to model the free-air gravity anomalies.

In order to estimate the densities for various litho logical units underlying the CIOB, the seismic velocities obtained for different geological horizons were used. Based on the correlation of observed seismic velocities with the mean Nafe-Drake curve, a three-layer density distribution is inferred for the underlying crust. Velocity data published by Curray et al., (1982), Neprochnov et al., (1988), and Popov (as discussed by Subrahmanyam and Singh, 1992) were considered in the present study for the purpose.

Giving details of the successive investigations made on the seismic velocity for the mid-plate deformation, Neprochnov et al., (1988) proposed three models, namely, (i) average model, (ii) model for monotonously deformed area and (iii) model for intensely folded and fractured anticlinal basement rise. For the average model, a typical three layered crust is inferred from seismic refraction data. Accordingly, sediments are 2.7km thick and the average thickness of the second layer with P wave velocity of 4.4km/sec to 5.1km/sec is 1.5km. The third layer of the oceanic crust with P wave velocity of 6.2 km/sec to 6.8km.sec is 3.5 to 6.7 km thick. The P wave velocity of the Moho is 8.0km/sec. For the monotonously deformed area of the CIOB, refraction data revealed anomalous features in the crustal structure. It comprises of weakly deformed sections of the basin with a smooth sea floor. It is made up of three layers which are chacterised by P wave velocities of 1.8km/sec to 2.0km./sec, 5.6km/sec and 6.6km/sec having thicknesses of 1.6km, 1.6km and 4.6km respectively. The seismic velocity of Moho is 8.2km/sec. For the model of intensely folded and fractured anticlinal basement rise (near 80^0E and 4^0S),

layers with P wave velocities of 2.0km/sec, 6.1km./sec, 6.9km/sec and 7.7km/sec are 1.1km, 1.3 km, 4.2 km and 6.6 km thick respectively. Neprochnov et al., (1988) viewed the 7.6km/sec layer as made up of unconsolidated upper mantle. In a generalized seismic profile between DSDP sites 218 and 215 near 2^0N and 2.5^0N Curray et al.,(1982) inferred two seismic columns with similar results of a layer of 7.6km/sec underlying layers with velocities of 7.0km/sec and 6.9km/sec.

Densities for the crustal models in the present investigation are based on the models of monotonously deformed area and intensely folded and fractured anticlinal basement described by Neprochenov et al., (1988). The densities used for water, sediments, oceanic crust and mantle are 1.03g/cc, 2.10g/cc, 2.84g/cc and 3.4g/cc respectively. Intermediate layers overlying the mantle are considered as having densities of 3.14g/cc and 3.24g/cc representing serpentinised plastic material of different composition.

MARINE GRAVITY AND MAGNETIC PROFILES

Free-air gravity and total field magnetic data of the CIOB were procured from the World Data Centre, Moscow, Russia in MGD77 format by second author (SR). The data supplied in analog form were digitized at an interval of one nautical mile. Fig.1 gives the layout of two N-S (AB and CD) and one E-W (EF) gravity profiles. Dashed line (GH) is the magnetic profile. Figs.2 and 3 show free-air gravity anomaly profiles along 79^0E and 81^0E longitudes respectively. The length wise extension of these profiles is from 1^0S to 13^0S latitudes. Fig.4 shows free-air gravity anomaly profile in the W-E direction along 7^0S latitude between $74^030^{'}$E to 80^0E longitudes. Fig.5 shows N-S trending magnetic anomaly profile along 80^0E longitude. Short wave length free-air gravity anomalies of considerable amplitude are more pronounced on the N-S profiles compared to the E-W profile. Free-air gravity anomaly profile along 79^0E longitude (Fig.2) is characterized by short wavelength (with amplitude 30-80 mgal) anomalies beyond 5.5^0S. Other notable features are a gentle gradient showing decrease of about 80 mgal upto about 5^0S and the anomaly at 5.5^0S position characterized by a steep rise of about 150 mgal. Indrani fracture crosses the profile in the vicinity of 4^0S. Disturbed basement associated with this feature could be inferred since the profile runs along the flanks of the fracture zone which makes an angle of about 5^0 with the profile. Bull (1990) identified the Indrani fracture and three other principal faults from multichannel seismic surveys. Fig.3 shows the free-air gravity anomaly profile along 81^0E longitude which is characterized by small rises and lows between 1^0S and 5.5^0S superposed on a regional trend that falls by 80 mgal over this segment. Beyond 5.5^0S there is a steep rise in the anomaly. Between 5.5^0S and 10^0S, the anomaly pattern is characterized by short wavelength anomalies of considerable amplitude (about 50 mgals) suggesting tectonic deformation of the basement involving domal rises. A sharp anomaly at about 10.5^0S position and a steep gradient beyond 11.5^0S position are notable. Basement highs and troughs inferred in the processed multichannel seismic records by Bull and Scrutton(1992) agree with the basement features of the crustal sections along 79^0E and 80^0E (Figs.2 and 3). Free-air gravity anomaly profile along 7^0S latitude (Fig.4) revealed a highly subdued folded geometry/arching as inherited from the outer layers of the lithosphere in response to block faulting and fracturing. In this

profile, sedimentary layer is absent. At about 77^0E and 78^0E positions the steep gradients coincide with a near north-south trending short fracture and Indrani fracture lineaments respectively (Fig.1). The sharp anomaly gradient at 79.5^0E coincides with another fracture zone (Fig.1). Magnetic data is available along 80^0E longitude lying in between the two gravity profiles. Limits of the magnetic profile are 1^0S and 9^0S latitudes. The variation in the magnetic anomalies is more pronounced with considerable amplitudes beyond 5^0S suggesting tectonic deformation of the basement. At 5.5^0S position the anomaly is indicative of faulting with possible shearing and magma tic intrusions. Similar disturbed conditions are noticed at 3.5^0S position. These characteristics and causative features are in common with the free-air anomaly profile and the corresponding crustal model along 79^0E longitude profile shown in Fig.2. The crustal models presented in Fig.2, 3 and 4 supports the view of Bull, Martinod and Devy (1992) about the model of deformation with the brittle layer above a ductile layer as explaining buckling of the entire brittle layer. The findings of the present investigation are in general agreement with the nature of faulting of basement inferred by Krishna et al.(1998) for a SE-NW processed multichannel seismic record between $01^009.55^'$S latitude $81^025.03^'$E longitude and $0^003.60^'$N latitude $80^054.97^'$E longitude.

CRUSTAL MODELS DERIVED FROM FREE-AIR GRAVITY AND MAGNETIC DATA.

Two N-S trending gravity profiles along 79^0E and 81^0E longitude between 1^0S and 13^0S latitude and an E-W trending gravity profile along 7^0S latitude between 74^0 30'E to 80^0E longitude have been interpreted in terms of crust-uppermost mantle structure. SAKI program of USGS software package (Mike Webring, 1985, USGS open-file report of 85-122) has been used for modeling the crust. Optimization is based on Marquardt's method. To begin with, the effect of water and sedimentary layers have been replaced by the effect of oceanic crust by considering the density contrast for water layer as 1.81 g/cc (2.84-1.03) and for sedimentary layers as 0.74 g/cc (2.84-2.10). Very thin sediment cover was noticed south of 7^0S from seismic reflection data (Krishna et al., 1998). The resulting curve corresponds to a two layer configuration of 2.84g/cc and 3.4g/cc densities and is interpreted in terms of crust-mantle model with material of intermediate nature in between. This is taken as the initial model for computing theoretical gravity anomalies to fit the observed free-air anomalies. Figs 2, 3 and 4 show the best fit models and the corresponding synthetic free-air gravity anomaly curves. For the crustal models, effect of water, sediments, oceanic crust, plastic layer and mantle have been incorporated and the body parameters and densities refined   to arrive at the best fit curves. From the nature of anomalies observed, and considering all the available information on the oceanic lithosphere processes, the models shown in Figs 2, 3 and 4 are found to be reasonable. Many attempts with different densities and geometry of the model have been made. Any change in geometry and/or density of the fault feature at 5.5^0S position in Figs.2 and 3 changed the synthetic curves considerably from the observed profiles. For interpreting the central portions of profiles in Figs.2 and 3 which are more disturbed, a number of intrusives or block dislocations were considered.   The resulting variation in the crustal and sub-crustal configuration indicates the possibility of wide lateral and vertical propagation of plastic material within the crust, as may be inferred from the models of Figs.2, 3 and 4 because of possible buckling of the oceanic

lithosphere resulting from N-S compression. Figs.2 and 3 indicate that the crust in the intensely deformed segment is made up of faulted blocks in the form of arching of the crust between 5.5^0S and 10.5^0S positions.   Depth to Moho increases from about 18.5km near 1^0S to about 23km near 5^0S in the case of 79^0E profile (Fig.2) and it increases from about 18km near 1^0S to about 21km near 5^0S in the case of 81^0E profile (Fig.3). Arching of the Moho between 5^0S and 10.5^0S is common to both the profiles. A prominent root-like feature in the oceanic crust reflected in the 81^0E profile is probably caused by faulting and vertical movement of blocks that extend deep into the mantle. The feature is not so significant in 79^0E profile (Fig.2). Another significant feature common to both the profiles is the sharp anomaly rise near 5.5^0S and the causative faulted structure with the lower elements extending into the mantle. This subduction-like feature trending in a near E-W direction and supporting the adjacent minor arching regime is actually associated with the higher seismicity observed in the zone of the sublatitudinal trend between 2^0N and 5^0N as pointed out by Levchenko(1989). The E-W trending free-air gravity anomaly profile along 7^0S latitude between Chagos-Laccadive Ridge ($74^0 30^{'}$E longitude) and 80^0E longitude is shown in Fig.4. Sedimentary layer is absent in this section. Although the attitude of the deformation zone is different from the trend of this profile a highly subdued folded geometry/arching is apparent in the outer layers of the lithosphere. The Moho depth increases from 21km near $74^0 30^{'}$E to about 25km near 80^0E. The depth decreases to 19km between 77^0E and 79.5^0E positions (Fig.4).

The total intensity magnetic anomaly profile has been divided into small segments for determining average spectral depths. The data of each segment has been subjected to Werner deconvolution. High frequency component was removed to obtain the depths to Curie Point isotherm. The inverse transform of the filtered signal was again subjected to Werner deconvolution to get the depth section to deeper marker. The depths thus determined to shallow and deeper markers have been used as initial depths to model the anomaly profile. Fig.5 shows the observed magnetic profile, best fit anomaly curve and the causative magnetic crust. The shallow interface corresponds to the surface of the basalt oceanic crust and the deeper interface corresponds to the Curie temperature isotherm or a lithologic change. The magnetic crust thus modeled is found to be in agreement with the oceanic crust as modeled from free-air gravity anomaly profiles and more particularly that of Fig.2. Figs. 2, 3, 4 and 5 suggest that the oceanic basement and the Moho boundary are highly irregular surfaces because of the deformation.

DISCUSSIONS

Crustal models worked out for the deformation zone reflected relative displacement of the oceanic crustal elements aided by faulting, folding and /or shearing involving thickening or thinning of plastic medium of density 3.14g/cc to 3.24g/cc in between the crust and the mantle. The findings suggested that the oceanic crust, besides assuming an arch-like (anticlinal rise) disposition in the highly disturbed segment, is found to be underplated by 3.14g/cc to 3.24g/cc density material which corresponds to P wave velocity of 7.2km/sec to 7.6km/sec. Neprochenov et al., (1988) viewed this layer as unconsolidated mantle in their model of intensely folded and fractured anticlinal basement rise in the vicinity of 4^0S and 80^0E. Material in this layer probably is serperntine as per the two level plate tectonic concepts proposed

by Verzbhitsky and Lebkovshy (1993) because P wave velocities of 7.2 km/sec to 7.6km/sec indicate serpentinized peridotite (Le Pichon et al., 1972). Serpentinisation is essentially one of auto metamorphism by later stage hydrothermal action on ultra basic rocks. Sea water can penetrate to uppermost mantle and hydrate the olivine which is the main constituent of peridotite, transforming it to serpentine which deforms plastically at moderate temperatures.

Exothermic reaction of serpentinisation due to lithopsheric fracturing and water penetration into the upper mantle might have caused strong heat flow anomaly in the intraplate deformation zone. Infact, the heat flow of CIOB is not homogeneous but shows strong scatter of values even at a distance of only a few kilometers. Largest values of 166 and $133 mW/m^2$ were observed in association with a basement fault (Cochran et al., 1988). Sychev et al., (1987) proposed the idea of wide lateral propagation of magma intrusions in the lower and upper parts of the crust of the CIOB and attributed it as the cause of anomalous heat flow. The motion of subcrustal lithosphere relative to upper crust produces dissipative heating of the lower crust and upper mantle that could cause an increase of the magnitude of the geothermal field of the CIOB. Any excess heat flow might result from a transient heat source, such as an intrusion of hot material within the lithosphere. Verzhbitsky and Lobkovsky (1993) suggest that the tectonic deformation in the CIOB after continent – continent collision took place mainly in the crustal levels, while the mantle part of the lithosphere slips under the crust of the Indian Ocean and the Indian subcontinent. It is clear that the basement forms a blocky structure because of brittle failure of the crust under N-S compressive forces. One possible source of the additional heat flow may be thermal energy released during the whole lithosphere folding caused by strong horizontal compression as pointed out by Weissel et al., (1980) and Stein et al., (1988). It may be pointed out here that earthquakes generally occur at depths where the temperatures are less than or equal to 750^0C. The earthquakes in the CIOB are of shallow type (Bergman and Soloman, 1985; Stein and Weissel, 1990). Seismicity in the intensely deformed zone led Levchenko (1989) to suggest that the deformation activity could be episodic in nature. The deformation which occurred at regular intervals appears to coincide with the release of thermal energy by upwelling of hot fluids.

The rationale in using two layers of density 3.14g/cc and 3.24g/cc in between the basaltic layer and upper mantle may be explained in the light of periodic instability of the lithosphere resulting in deformation in the late Miocene and the late Pliestocene in the area south of 1^0S latitude thus: Seismic reflection records (Krishna et al., 1988) revealed deformation of oceanic basement and overlying sedimentary strata in the latitudinal stretch between 10^0S and 7^0N. Three significant seismic boundaries were recognized in the sedimentary section. The oceanic basement and the sediment section below the lower boundary are found to be crumpled at several locations in the form of tight folds and high angle faults indicating the occurrence of intense deformation. Correlation with results of ODP Leg 116 sites and DSDP site 218 suggested an age of 7.5 Ma (upper Miocene) to the boundary. Sediments lying to the NW of the ODP Leg 116 sites are found to be disturbed at the time of the formation of middle boundary suggesting reoccurrence of deformation activity after the formation of the middle boundary which coincides with the age of early Pliocene (4.0Ma) and represents another compressional stress regime

(Cochran et al., 1989). The upper boundary when correlated with results of ODP Leg 116 sites indicated upper Pleistocene (0.8 Ma).

Periodic instability of the lithosphere finds expression in the intensely disturbed crustal sections (Fig.2, 3, 4 and 5) with attendant deformation of the overlying sediments and also in the underlying plastic layers and uppermost mantle. The instability that developed during the Indian plate collision with Eurasian plate was intensified further during the evolution of the Himalayas resulting in a number of major tectonic events in the Indian Ocean. After the Himalayas came into being, the deformation activity was reset at 7.5Ma in the Central Indian Ocean Basin and again at 0.8Ma in the area south of 1^0S (Krishna et al., 1998). These events of late Miocene (~7.5Ma) and late Pliestocene (~0.8Ma) deformed the oceanic lithosphere intensively and the results of the present investigation lend ample support. The intermediate layers of 3.14g/cc and 3.24g/cc density postulated here provide the necessary means for upward penetration and fracturing the oceanic crust repeatedly, creating arched structures. The interaction of seawater with peridotite of the uppermost mantle alters it into serpentine which is much less denser than peridotite and more plastic, so that it can be squeezed up towards the surface along fractures in the crust. Saturation of the lower crust with mantle material in the process of general depression is also possible. These two may explain the relevance of density variation of the plastic layer as 3.14g/cc and 3.24g/cc in the light of the deformation activity after the Himalayas came into being in the late Miocene and late Pliocene.

CONCLUSIONS

Free-air gravity anomaly profiles along 79^0E and 81^0E longitudes between 1^0S and 13^0S latitudes revealed that the crust in the intensely deformed segment is made up of faulted blocks indicating arching of the crust, particularly between 5.5^0S and 10.5^0S latitudes. The steep gradient observed at 5.5^0S is modeled as due to a faulted structure with its lower elements extending into the mantle.

The W-E trending free-air gravity anomaly profile revealed a highly subdued folded geometry because the attitude of the deformation zone makes a small angle with the orientation of the profile.
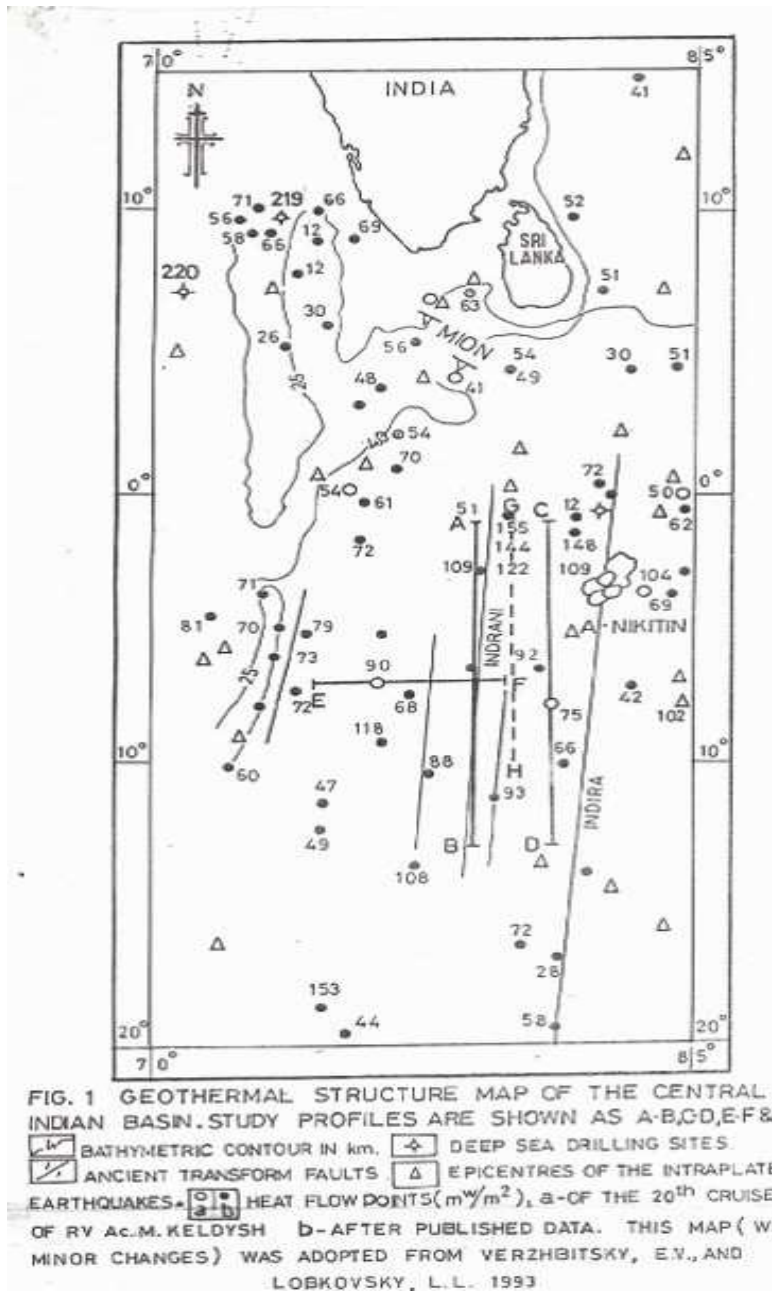
Total intensity magnetic anomaly profile along 80^0E longitude between 1^0S and 9^0S latitudes resulted in a crustal model which is found to be in general agreement with the models deduced from free-air gravity anomalies and more particularly, that of 79^0E profile.

Crustal modeling suggested that the oceanic crust is found to be underlain by 3.14g/cc to 3.24g/cc density material which corresponds to P wave velocity of 7.2km/sec to 7.6km/sec. indicating serpentinised peridotite. Levchenko`s (1989) observation that the deformation activity could be episodic in nature supports the situation that the deformation occurring at regular intervals coinciding with the release of thermal energy by upwelling of hot fluids. The instability developed in the Indian Ocean because of the Indian plate motion and subsequent collision followed by two events of late Miocene (~7.5Ma) and late Pleistocene (~0.8Ma) are explained as causing deformation in the Central Indian Ocean Basin region south of 1^0S.

REFERENCES

1. Bergman,   E.A., and Solomon, S.C., 1985, Earthquake source mechanisms from body Wave inversion   and intra-plate tectonics in the Northern Indian Ocean. .Physics of the Earth and Planetary interiors, 40, 1 – 23.

2. Bull, J.M. (1990). Structural style of intraplate deformation, Central Indian Ocean basin: Evidence for the role of fracture zones, Tectonophysics, 184,213-228.

3. Bull, J.M. And Scrutton,   R.A., 1990, Fault reactivation in the Central Indian Ocean and rheology   of the oceanic lithosphere, Nature, 344, 855-858.

4. Bull, J.M. and Scrutton,   R.A., 1992. Seismic reflection images of intraplate deformation, Central Indian Ocean and their tectonic significance.J.Geol.Soc.London, 149, 955-966.

5. Bull, J.M., Martinod, J and Davy, Ph., 1992. Buckling of the Oceanic lithosphere from Geophysical data and experiments. Tectonics, 11, 537-548

6. Cochran,   J.R., Stow, D.A.V., et al., 1988, Intraplate deformation and Bengal Fan sediments: background and objectives. Proc. Ocean Drilling Program. Initial reports. 116, College Station, TX, 116, 3-11.

7. Cochran, J.R., 1990. Himalayan uplift, sea level, and the record of Bengal Fan sedimentation at the ODP Leg 116 Sites, In Cochran, J.R., Stow, D.V.V et al., Proc.Sci.Results, 116: College Station, TX (Ocean Drilling Programme), 397-414.

8. Curray, J.R. and Moore, D.G., (1971) Growth of the Bengal deep sea Fan and denudation in the Himalayas.Geol.Soc.Am.Bull. 82,563-572.

9. Curray J.R, Emmel, F.J., Moore, D.G.   And Raitt, R.H. (1982) Structure, tectonics and geological history of the north – eastern Indian Ocean: In: The Ocean Basin and Margins.   eds. A.E.M.Nairn and F.G.Stehli, vol.6, The Indian Ocean, Plenum Publ.corpn., 399-450.

10. Curry, J.R. and Munising, T. (1989). Timing of intraplate deformation, northeastern Indian Ocean. Earth and Planetary Science Letters, 94, 71-77.

11. Eittreim, S.L., and Ewing, J., 1972, Mid-Plate Tectonics in the Indian Ocean; Jour. Geophys. Res., 32,   6413 – 6421   Plateau, Western Indian Ocean; Geol. Soc. Amer. Bull, 78, 1247-1266.

12. Krishna, K.S., Ramana, M.V. and GopalaRao, D, and Murhty, K.S.R, Malleswara Rao, M.M., Subrahmanyam, V and Sarma, K.V.L.N.S. (1998). Periodic deformation of oceanic crust in the Central Indian Ocean. Journal of Geophysical Research, 103, 17859-17875.

13. Lepichon X., Francheteau J. And Bonnin J. 1972. Plate tectonics J.R. Astron.Soc., 26,   515-535.

14. Levchenko, O.V., Merklin, L.R., and Neprochnov, Yu.P. (1985). The folded features in the Central Indian Basin. Geotechnica, 1, 15-23(in Russian).

15. Levchenko, O.V., 1989, Tectonic aspects of intraplate seismicity in the northeastern Indian Ocean; Tectonophysics, 170, 125 - 139.

16. Mike Webring, 1985, U.S. Geological Survey open file report of 85 - 122.

17. Murthy, K.S.R., Yu.P.Neprochnov, Levchenko, O.V., Rao, T.C.S, VE Milanovsky and Lakshminarayana, S. 1993. Some new observations on the intraplate deformation in the Central Indian Ocean (CIB). Mar.Geol. 114, 185-193.

18. Nafe, J.E and Drake, C.L. (1963) Physical properties of marine sediments In: M.N.Hill (Ed). The sea, Wiley. NY, 3, 794 - 815.

19. Neprochnov,   Yu.P, Levchenko. O.V., Merklin, L.R. And Sedov, V.V., 1988, The Structure and tectonics of the intraplate deformation area in the Indian Ocean, Tectonophysics, 156, 89 - 106.

20. Popov, A.A. (1986) Seismic measurements in Indian Ocean, Unpublished Ph.D. Thesis (in Russian).

21. Stein, C.A.,   and Jeffrey K. Weissel, 1990, Constraints on the Central Indian Basin thermal Structure from heat flow, seismicity and bathymetry, Tectonophysics, 176, 315 - 332.

22. Stein, C.A., Cloetingh, S. and Wortzel, R. (1989). Seasat derived gravity constraints on stress and deformation in the northeastern Indian Ocean. Geophysical Research Letters, 16,823-826.

23. Stein, C.A., Hobart, M.A., and Abbott, D.H., (1988). Has the Wharton Basin's heat flow been perturbed by the formation of a diffuse plate boundary in the Indian Ocean?. Geophy.Res.Lett, 15, 455-458.

24. Subrahmanyam, C. and   R.N. Singh. (1992) Geotectonics of the Bay of Bengal. Indian Journal of Petroleum geology, 1 (2), 161 - 180.

25. Sychev, P.M.Vorobev V.M., Lyutaya, L.M., Patrikeev, V.N., Popov, A.A., Reverdatto, V.V. and Soinov, V.V. 1987. Folded deformations of the sedimentary Cover in the South – Western Bengal Bay. Tikhookeanskaya Geologiya, 25- 36 (in Russian).

26. Verzhbitsky, E.V., and Lobkovsky, L.I., 1993. On the Mechanism of heating up of the Indo – Australian Plate, Jour. Of Geodynamics, Vol, 17, No. ½, May/June 1993, 27 - 38.

27. Weissel, J.K., Anderson, R.N. and Geller, C.A., 1980 Deformation of the   Indo - Australian plate, Nature, 287, 284 - 291.
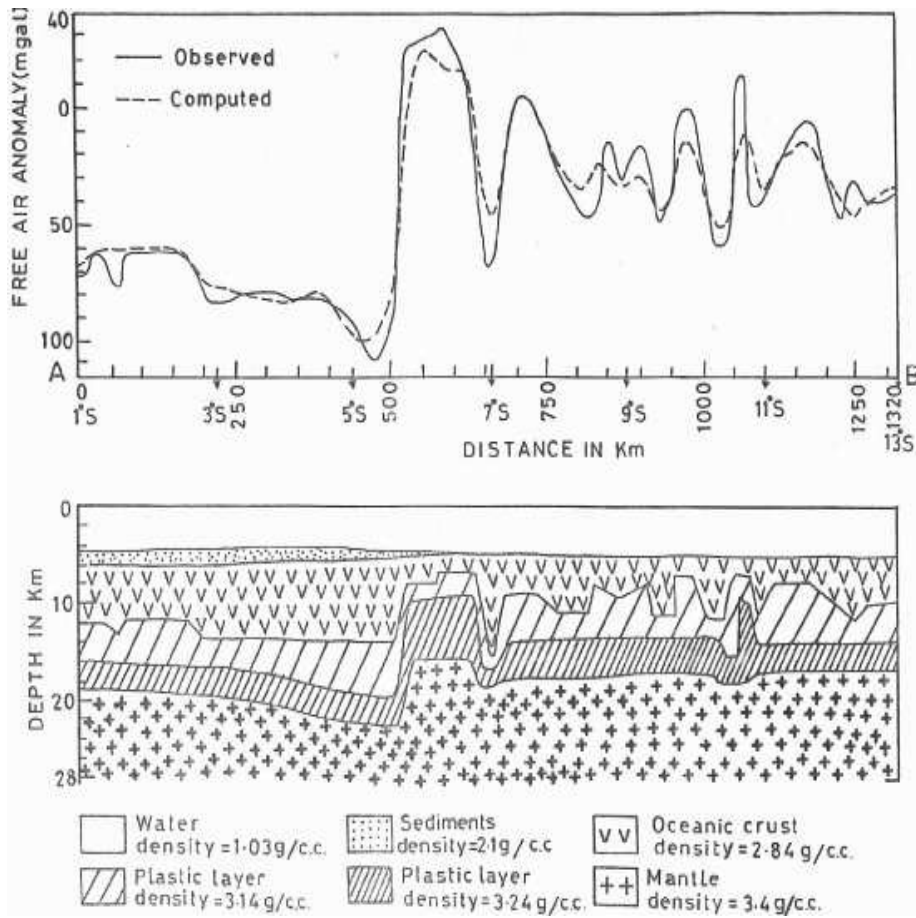
FIG. 1 GEOTHERMAL STRUCTURE MAP OF THE CENTRAL INDIAN BASIN. STUDY PROFILES ARE SHOWN AS A-B,CD,E-F&G BATHYMETRIC CONTOUR IN km. DEEP SEA DRILLING SITES. ANCIENT TRANSFORM FAULTS. EPICENTRES OF THE INTRAPLATE EARTHQUAKES. HEAT FLOW POINTS(m^w/m^2), a-OF THE 20th CRUISE OF RV Ac.M.KELDYSH b-AFTER PUBLISHED DATA. THIS MAP (WIT MINOR CHANGES) WAS ADOPTED FROM VERZHBITSKY, E.V., AND LOBKOVSKY, L.L. 1993

**Figure 2.Free-Air Gravity Anomaly Profile(Ab) as Shown In Fig.1 Along with Computed Curve
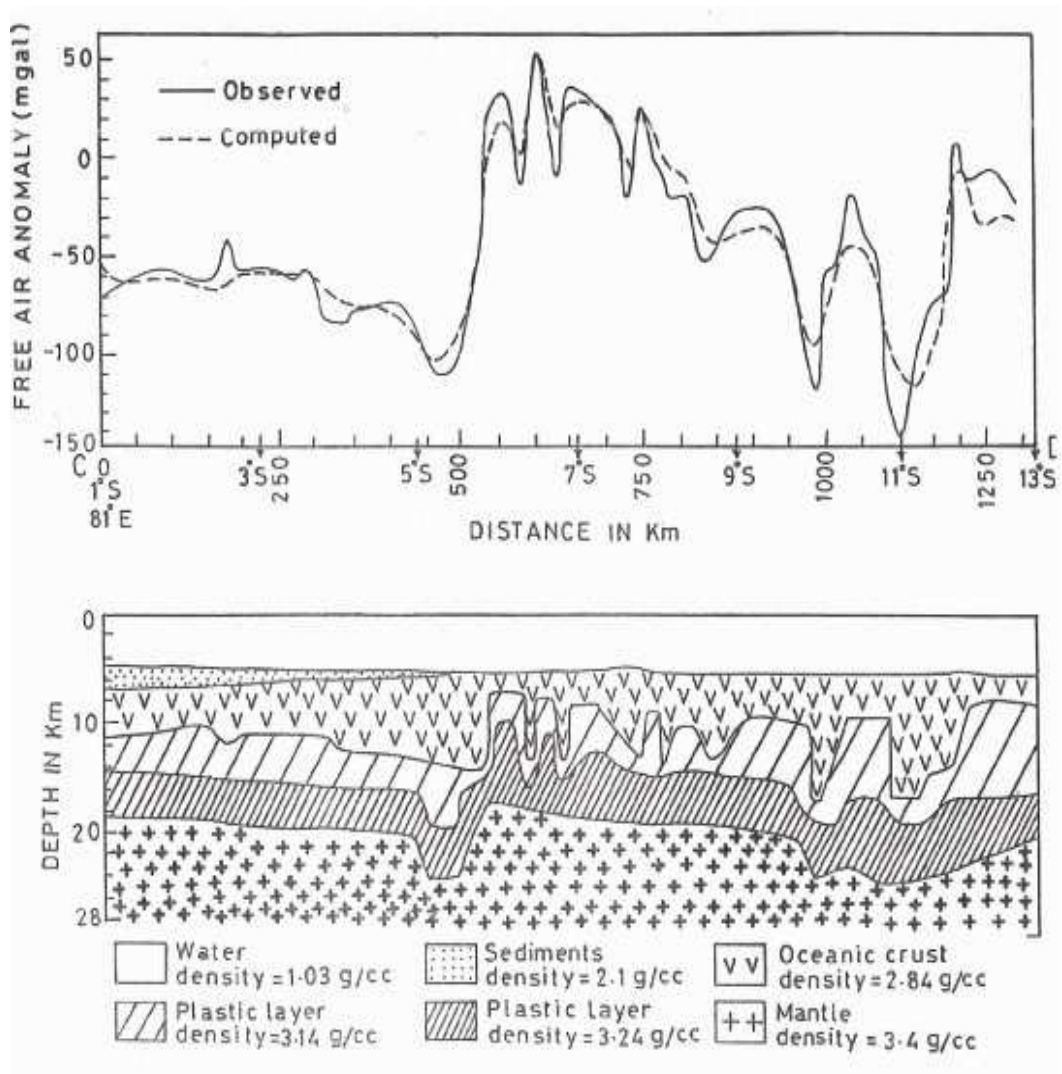and the Best Fit Crustal Mosel.**

Figure 3. Free-Air Gravity Anomaly Profile(Cd) as Shown In Fig.1 Along with Computed Curve and the Best Fit Crustal Model.
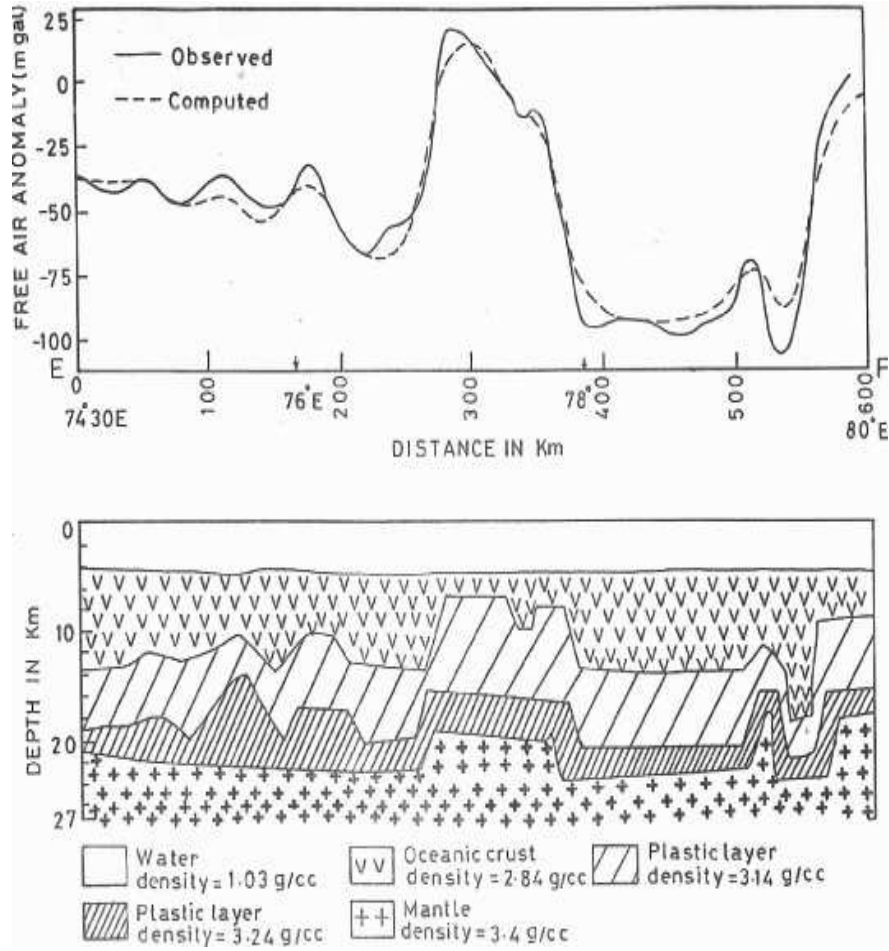
Figure4. Free-Air Gravity Anomaly Profile(Ef) as Shown In Fig.1 Along with Computed Curve and the Best Fit Crustal Model.
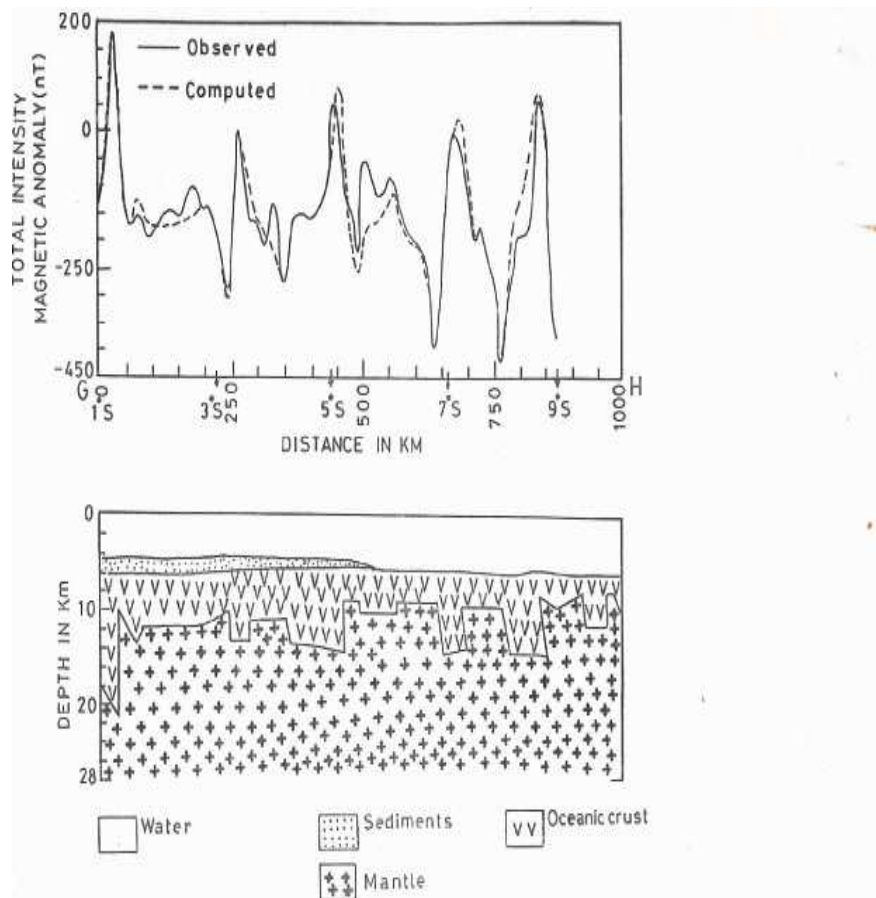
Figure 5. Total Intensity Magnetic Anomaly Profile (Gh) as Shown In Fig.1 Along with Computed Curve and the Best Fit Crustal Model.